ACS APPLIED MATERIALS & INTERFACES

Research Article

www.acsami.org

Nickel–Cobalt Oxide Decorated Three-Dimensional Graphene as an Enzyme Mimic for Glucose and Calcium Detection

Meiyan Wu, Shangjun Meng, Qian Wang, Weili Si, Wei Huang,* and Xiaochen Dong*

Key Laboratory of Flexible Electronics (KLOFE) & Institute of Advanced Materials (IAM), Jiangsu National Synergistic Innovation Center for Advanced Materials (SICAM), Nanjing Tech University (Nanjing Tech), 30 South Puzhu Road, Nanjing 211816, China

ABSTRACT: Glucose and calcium ion play key roles in human bodies. The needlelike $NiCo_2O_4$ nanostructures are in situ deposited on three-dimensional graphene foam (3DGF) by a facile hydrothermal procedure. The structure and morphology of the hierarchical $NiCo_2O_4$/3DGF are characterized by scanning electron microscopy, transmission electron microscopy, and X-ray diffraction. With the self-standing $NiCo_2O_4$/3DGF as electrochemical electrode, it can realize the high-sensitivity detections for glucose and calcium ion. The limit of detection can reach 0.38 and 4.45 μM, respectively. In addition, the electrochemical electrode presents excellent selectivity for glucose and calcium ion. This study demonstrates that $NiCo_2O_4$/3DGF is a unique and promising material for practical application in both glucose and calcium ion sensing.

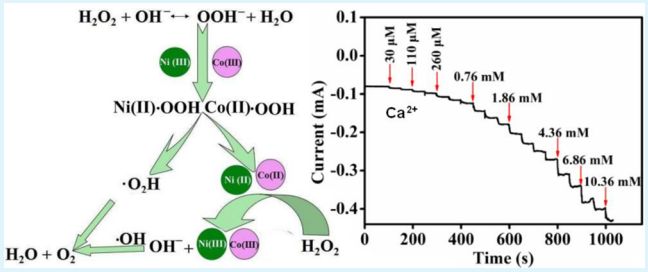

KEYWORDS: *cobalt nickel oxide, 3D graphene, sensitivity sensing, glucose, calcium ion*

INTRODUCTION

Diabetes has become one of the biggest global threats to human health. The blood glucose level is the most representative characteristic of this disease, including type 1 and type 2 diabetes.[1] To measure the blood glucose level, the development of glucose sensor has been greatly encouraged, especially in the field of nanotechnology.[2] Tremendous efforts have been put into developing low-cost, high-sensitivity, and excellent selectivity glucose sensors[3] since the natural enzymes applied in conventional sensors have several drawbacks, like low stability and high cost. On the other hand, calcium ion also plays a vital role in human blood for maintaining various physiological functions of the human body. A large number of diseases are related to the concentration of Ca^{2+} in the blood, such as secondary hyperparathyroidism (SHPT),[4] pheochromocytoma (PHEO), and hypocalcemia. Therefore, detecting the concentration of calcium ion is of great importance in biological and clinical analysis and more works need to be done for limitation of the determination of calcium ion.

It has been demonstrated that nanostructured transition-metal oxides are applicable to the fabrication of enzyme-free glucose sensors,[5−10] supercapacitors,[11,12] energy storage,[13,14] or lithium-ion battery[15] owing to its attractive shape, unique size, and high stability. Recently, nanomaterials including Pt,[16] Fe_3O_4,[17] and Co_3O_4[18] nanoparticles as enzyme mimics have received increasing attention. In addition, the spinel compounds of AB_2O_4 have attracted tremendous interest due to their fascinating magnetic, optical, electronic, and catalytic properties.[19−21] Among these spinel-type oxides, $NiCo_2O_4$ has been investigated as alternative materials because of their low cost, flexible ion exchangeability, great electrochemical performance, and high natural abundance. $NiCo_2O_4$ also exhibits synergistic enhancement in electrocatalytic activity, which is much better than the simple combination of nickel and cobalt oxides.[22]

Graphene, a two-dimensional carbonaceous material, has been widely applied in sensors,[23] supercapacitors,[24] catalysis,[25] drug delivery,[26] and flexible optoelectronics[27] owing to its outstanding electronic conductivity, large specific surface area,[28] mechanical strength, flexibility, and great optical properties.[29] It is well-known that the reduced graphene oxide (rGO) shows a lot of defects and chemical moieties created in the synthesis process. Moreover, the strong $\pi-\pi$ interaction between individual graphene sheets leads to aggregation and stacking of the rGO, which makes its specific surface area decrease greatly. In contrast, three-dimensional graphene foam (3DGF) synthesized by chemical vapor deposition (CVD) can effectively improve the stability of the structure and provide large porous structure with high conductivity. Therefore, the high-performance carbon-based composites for electrochemical sensors can be fabricated with hierarchical and porous structure.

In this work, 3DGF with high conductivity and large specific surface area was synthesized by the CVD method. Then, $NiCo_2O_4$ nanoneedles were deposited onto its surface by a hydrothermal approach. On the basis of the unique electrochemical behavior of the free-standing $NiCo_2O_4$/3DGF electrode, an electrochemical sensor was designed for the detection of glucose and calcium ion. The synergistic effect between graphene and $NiCo_2O_4$ makes the $NiCo_2O_4$/3DGF

Received: May 17, 2015
Accepted: September 2, 2015
Published: September 2, 2015

DOI: 10.1021/acsami.5b06299
ACS Appl. Mater. Interfaces 2015, 7, 21089−21094

electrode present high sensitivity, excellent selectivity, and low detection limitation.

EXPERIMENTAL SECTION

Materials. Nickel chloride hexahydrate ($NiCl_2·6H_2O$), cobalt chloride hexahydrate ($CoCl_2·6H_2O$), urea (CH_4N_2O), glucose, hydrogen peroxide (H_2O_2), Tris(hydroxymethyl)aminomethane ($C_4H_{11}NO_3$), dopamine (DA), ascorbic acid (AA), lactose, and D-fructose (D-F) were purchased from Aladdin (USA). All the reagents were used without any further purification.

Synthesis of $NiCo_2O_4$/3DGF. In this experiment, 3DGF was synthesized by chemical vapor deposition as described in our previous reports.[30] The $NiCo_2O_4$/3DGF was prepared via a simple one-step in situ hydrothermal method. Briefly, 20 mM $CoCl_2·6H_2O$, 40 mM $NiCl_2·6H_2O$, and 120 mM urea were added into 35 mL of deionized water under vigorous stirring for 10 min. Then the mixture was transferred into a 50 mL autoclave. The 3DGF fixed on a glass slide was immersed into the solution slowly, sealed, and maintained at 160 °C for 6 h. The composites were washed with deionized water and dried at 80 °C. Finally, the synthesized products were annealed at 400 °C for 3 h in air and $NiCo_2O_4$/3DGF was obtained.

Characterization. The morphology of $NiCo_2O_4$/3DGF was observed with scanning electron microscopy (SEM, Hitachi S-4800) and transmission electron microscopy (TEM, JEOL JEM-2010). The X-ray diffraction (XRD) was carried out on a Bruker D8 Advanced Diffractometer using Cu Ka radiation with a scanning rate of 2° per minute.

Electrochemical Measurements. Cyclic voltammetry (CV) and amperometry measurements were performed using a CHI660D electrochemical workstation (Chenhua, Shanghai) with the three-electrode configuration. The $NiCo_2O_4$/3DGF served as the working electrode, while a platinum wire electrode and an Ag/AgCl electrode were selected as the counter and reference electrodes, respectively. NaOH solution (0.1 M) was used as the electrolyte in the detection of glucose, while 0.1 M Tris buffer acts as the electrolyte for calcium ion determination.

RESULTS AND DISCUSSION

Figure 1 shows the XRD patterns of the pure 3DGF and $NiCo_2O_4$/3DGF, respectively. The significant diffraction peaks

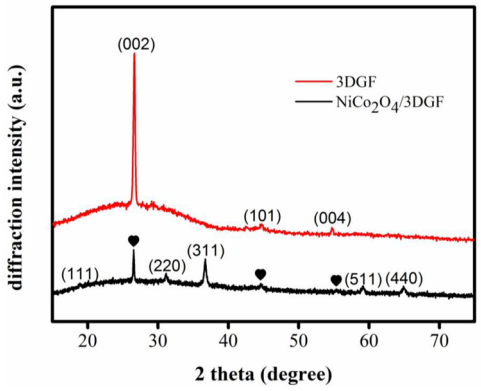

Figure 1. XRD patterns of 3DGF and $NiCo_2O_4$/3DGF.

of 3DGF at around 26.4°, 44.4°, and 54.5° can be indexed to the (002), (101), and (004) planes of graphitic carbon, respectively (JCPDS 41-1487). Besides the characteristic peaks of graphene, the significant peaks at around 2θ values of 18.9°, 31.2°, 36.3°, 59.1°, and 64.9° for $NiCo_2O_4$/3DGF were well-indexed to the (111), (220), (311), (511), and (440) planes of $NiCo_2O_4$ (JCPDS 73-1702), respectively. The XRD spectrum confirms the successful integration of $NiCo_2O_4$ and 3D graphene to form $NiCo_2O_4$/3DGF composite.

Figure 2 shows the morphologies of the $NiCo_2O_4$/3DGF characterized by SEM and TEM, respectively. It can be seen

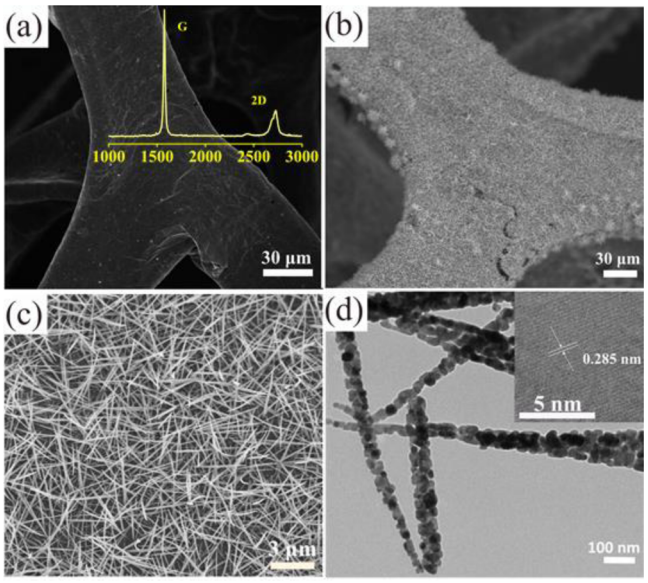

Figure 2. SEM images of 3DGF (a) and $NiCo_2O_4$/3DGF at different magnifications (b, c). The inset shows the Raman spectrum of 3DGF. (d) Low- and high-resolution (inset) TEM images of the nanoneedles deposited on 3D graphene.

that the naked 3D graphene foam presents porous structure with a smooth skeleton (Figure 2a). Furthermore, two prominent characteristic peaks at around 1560 and 2700 cm^{-1} have been presented by the Raman spectra of 3DGF (the inset in Figure 2a), corresponding to G and 2D bands of graphene, respectively.[31] The absence of the G band at around 1350 cm^{-1} indicates that the CVD-grown 3DGF has high quality and high conductivity. By the intensity ratio of the 2D and G peaks (0.55), the prepared 3DGF is composed of multilayered graphene.[32] After the formation of $NiCo_2O_4$/3DGF composite (Figure 2b), the skeleton of the porous 3DGF was uniformly covered by the $NiCo_2O_4$. The higher magnification SEM image (Figure 2c) reveals that the $NiCo_2O_4$ presents uniform needlelike morphology with diameter of around 25 nm. As shown in Figure 2d, the TEM image suggests that the nanoneedles are composed of numerous nanoparticles and the nanoparticles are linked together, which is useful for the enhancement of its specific surface area. High-resolution TEM in the inset of Figure 2d shows that the *d*-spacing of $NiCo_2O_4$ is around 0.285 nm, which is in agreement with the (220) planes of $NiCo_2O_4$ nanoparticles.

Glucose Sensing. The electrochemical performance of the $NiCo_2O_4$/3DGF electrode is measured in 0.1 M NaOH solution. As shown in Figure 3a, a couple of sensitive redox peaks can be observed at the potential of 0.35 and 0.5 V in the CV curves, respectively, which could be attributed to the redox reactions of Co and Ni species in the alkaline electrolyte corresponding to the following equations:[33−35]

$$NiCo_2O_4 + OH^- + H_2O \rightarrow NiOOH + 2CoOOH + e^- \quad (1)$$

$$CoOOH + OH^- \rightarrow CoO_2 + H_2O + e^- \quad (2)$$

Furthermore, the current peaks rise and shift with the increasing of scan rates. Figure 3b illustrates that both cathodic

DOI: 10.1021/acsami.5b06299
ACS Appl. Mater. Interfaces 2015, 7, 21089−21094

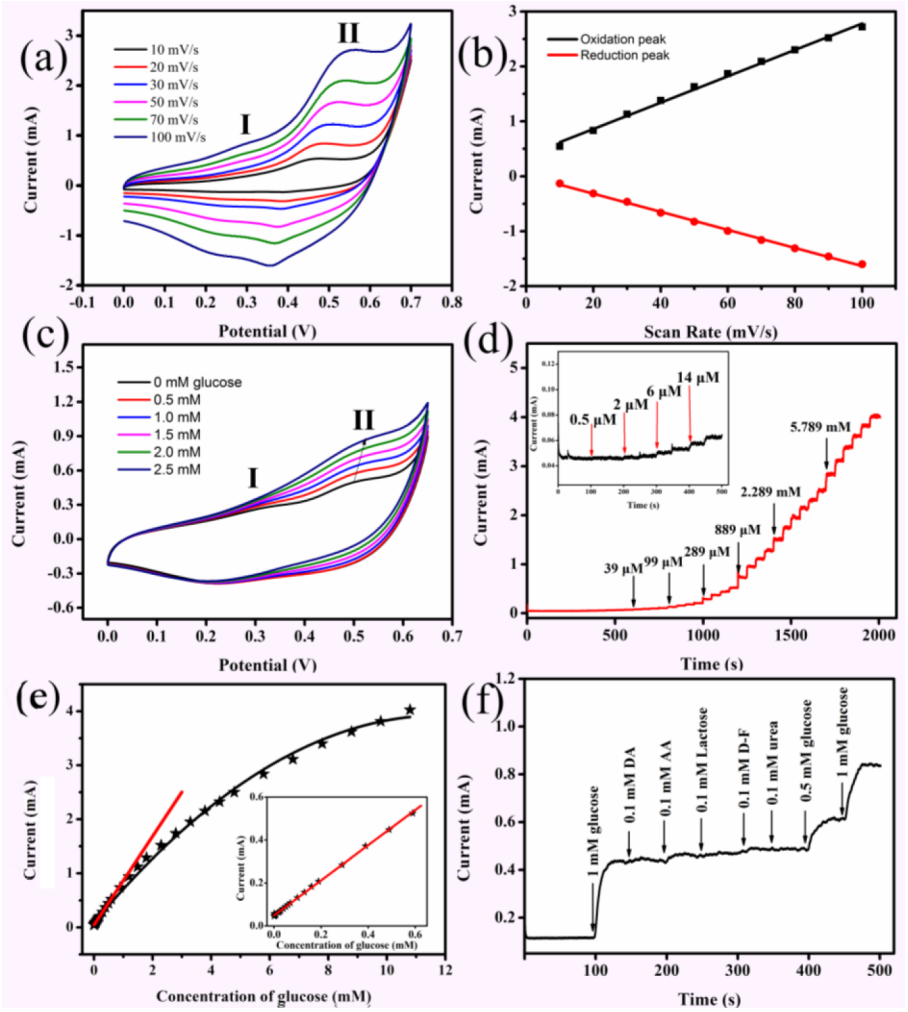

Figure 3. (a) CV curves of $NiCo_2O_4$/3DGF measured at different scan rates in 0.1 M NaOH solution. (b) Plots of redox peak currents versus scan rate. (c) CV curves in the presence of various concentrations of glucose. (d) Amperometric response of $NiCo_2O_4$/3DGF (at 0.5 V) upon successive addition of glucose. The inset shows the current response toward addition of 0.5−14 μM glucose. (e) Average dose response curve with a linear fitting at lower concentration range and a logarithmic fitting at a higher concentration range. The inset is the corresponding linear relation in the range from 500 nM to 1.489 mM. (f) Amperometric response to the addition of glucose, DA, AA, lactose, D(−)-fructose (D-F), and urea at 0.5 V.

and anodic peak currents of the $NiCo_2O_4$/3DGF electrode increase linearly with the scan rates, suggesting a surface-controlled electrochemical process of $NiCo_2O_4$/3DGF.[36] Figure 3c shows the CV curves of the $NiCo_2O_4$/3DGF electrode measured in the presence of glucose (scan rate of 50 mV s^{-1}). It can be clearly seen that the introduction of glucose (0, 0.5, 1.0, 1.5, 2.0, and 2.5 mM) makes an obvious increase of the redox peak currents (at ~0.5 and 0.3 V). This phenomenon can be ascribed to the glucose oxidation to gluconolactone, which is accompanied by the conversion of Co(IV) to Co(III) and Ni(III) to Ni(II):

$$\mathrm{Co(IV)} + \mathrm{Ni(III)} + \mathrm{glucose} \rightarrow \mathrm{Co(III)} + \mathrm{Ni(II)} + \mathrm{gluconolactone} \quad (3)$$

With increasing the glucose concentration, the anodic peak potential (II) shifts to a positive direction because of the oxidized intermediates and the absorption of glucose on the active sites of the electrode.[38] Moreover, the combination of nickel and cobalt makes the peaks potential (II) wider than nickel oxide electrode[39] or cobalt oxide electrode.[36]

Figure 3d shows the amperometric responses of the $NiCo_2O_4$/3DGF electrode to successive additions of glucose. With the addition of glucose, the current increases rapidly, indicating its excellent glucose detection performance. The corresponding calibration curve for glucose detection is plotted in Figure 3e. A linear concentration range from 500 nM to 0.59 mM (the magnified plot of this part is inserted in Figure 3e) with a slope of 818.51 μA mM^{-1} and a correlation coefficient (R^2) of 0.9999 is obtained from the curve. The sensitivity of the $NiCo_2O_4$/3DGF electrode is calculated to be as high as 2524 μA mM^{-1} cm^{-2}. When the concentration of glucose increases to 5.80 mM, it is found that the current response reaches saturation gradually, indicating that all active sites of the electrode are covered with reaction intermediates at high concentration of glucose. On the basis of the equation of S/N = 3 (signal-to-noise ratio = 3), the limit of detection (LOD) can reach up to 0.38 μM.

To investigate the selectivity of the $NiCo_2O_4$/3DGF electrode, the amperometric response upon the successive addition of 1 mM glucose, 0.1 mM dopamine (DA), ascorbic acid (AA), lactose, D-fructose (D-F), urea, and 0.5 and 1 mM glucose into 0.1 M NaOH at 0.5 V were also recorded (Figure

DOI: 10.1021/acsami.5b06299
ACS Appl. Mater. Interfaces 2015, 7, 21089−21094

3f). It can be seen that the current response of interfering compounds can be negligible, while remarkable current enhancements can be observed by the addition of glucose. Considering the concentration of glucose in human serum is 30 times higher than that of interfering species,[40,41] these results indicate that $NiCo_2O_4$/3DGF electrode has excellent selectivity for glucose detection and a promising future for practical applications. And remarkably, the $NiCo_2O_4$/3DGF electrode apparently outperforms the previously reported modified electrodes (Table 1).

Table 1. Comparison of the Properties of $NiCo_2O_4$/3DGF Electrode with Various Nonenzymatic Glucose Sensors Reported Previously

electrode	sensitivity (μA mM^{-1} cm^{-2})	detection limit (μM)	linear range	ref
Co_3O_4/3DGF	3390	0.025	up to 80 μM	36
$Ni(OH)_2$/3DGF	2650	0.34	1 μM to 1.17 mM	35
NiO-HMSs/GCE	2390	0.53	1.67 μM to 0.42 mM	37
$NiCo_2O_4$/Ni foam	91.34 mV/decade	1.49	0.005−15 mM	38
$NiCoO_2$/C/GCE	549.3	0.5	0.02−2.41 mM	39
$NiCo_2O_4$/3DGF	2524	0.38	0.5 μM to 0.59 mM	this work

Calcium Ion Sensing. With the existence of hydrogen peroxide, the sensing performance of $NiCo_2O_4$/3DGF electrode to calcium ion was investigated in Tris solution. Figure 4a records the CV curves of $NiCo_2O_4$/3DGF electrode in different concentrations of H_2O_2 at the scan rate of 50 mV s^{-1}. Also, the current response to the calcium ion with 5 mM H_2O_2 was measured. Obviously, with the increasing of H_2O_2 concentration, the current decreased correspondingly. The current decreases significantly, after the addition of 5 mM calcium ion (Ca^{2+}). The result implied that the addition of Ca^{2+} will bring greater current response. This phenomenon maybe comes from the fact that the calcium ion can stimulate the catalytic activity of cobalt ion as reported.[42]

It is well-known that cobalt ion in Co_3O_4 nanomaterials serving as a catalase mimic can catalyze the process of hydrogen peroxide decomposition. The catalytic activities and mechanisms have been investigated by Mu et al.[43] According to previous works,[43,44] a possible mechanism can be proposed as follows (Scheme 1): In the system, the concentration of perhydroxyl anion (OOH^-) is high because of the reaction between hydrogen peroxide with hydroxyl ion. The formed Ni(II)·OOH and Co(II)·OOH cause the decomposition of H_2O_2. Finally, the two kinds of ions turned back to Ni(III) and Co(III), indicating the nickel cobalt catalyzes the decomposition of hydrogen peroxide and decreases the CV current.

Figure 4b show the amperometric response curves of $NiCo_2O_4$/3DGF electrode to 0.3 mM Ca^{2+} in 0.1 M Tris base with 8 mM H_2O_2 at different potentials. It can be seen that the response curve at the potential of −0.6 V exhibits the

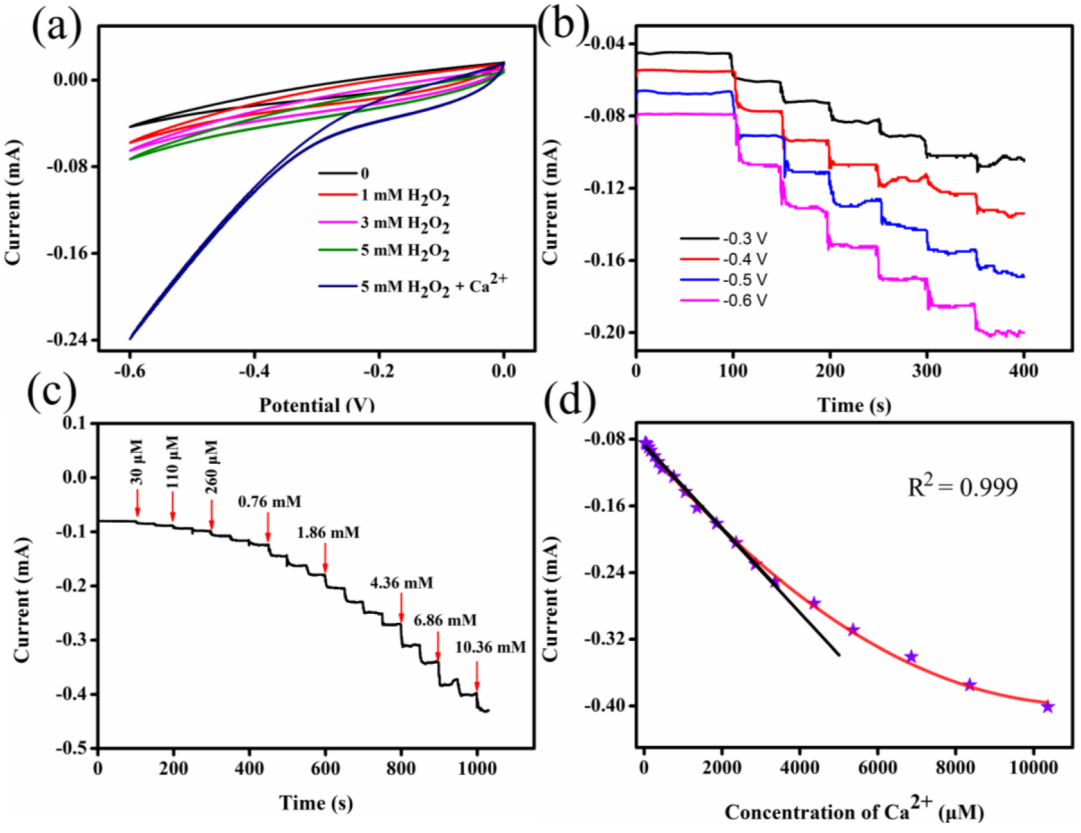

Figure 4. (a) CV curves recorded on different concentrations of H_2O_2 and with or without the addition of Ca^{2+}. (b) Amperometric response of $NiCo_2O_4$/3DGF upon successive addition of 0.3 mM Ca^{2+} at different potentials. (c) Amperometric response of $NiCo_2O_4$/3DGF upon successive addition of Ca^{2+} at the operating potential of −0.6 V. (d) Average dose response curve (amperometric current response vs Ca^{2+} concentration) with a linear fitting at lower concentration and an logarithmic fitting at higher concentration.

DOI: 10.1021/acsami.5b06299
ACS Appl. Mater. Interfaces 2015, 7, 21089−21094

Scheme 1. Proposed Mechanism of $NiCo_2O_4$ as Enzyme Mimic

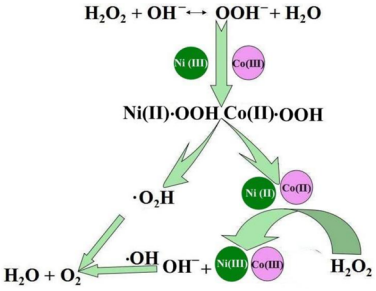

strongest response and excellent stability, indicating −0.6 V is the most appropriate potential for sensing. At the operating potential of −0.6 V, the amperometric response to the increasing concentrations of calcium ion is presented in Figure 4c. A well-defined, rapid current decreased and a stable curve can be observed after the addition of calcium ion, indicating the $NiCo_2O_4$/3DGF electrode presents a sensitivity and rapid response to calcium ion. The corresponding calibration curve is presented in Figure 4d. The average dose response demonstrates that a large concentration range can be made for detection, and a good linear dependence on the calcium ion concentration in the range of 30−460 μM with an exceptional sensitivity of 284.54 μA mM^{-1} cm^{-2} (R^2 = 0.999) is achieved. The limit of detection (S/N = 3) can be calculated as low as 4.45 μM. The sensing performances of linear range, detection limitation are excellent for the determination of calcium ion. The selectivity of the electrode for Ca^{2+} was also investigated against some metal ions normally existing in the human blood. Figure 5 showed the response of $NiCo_2O_4$/3DGF electrode for

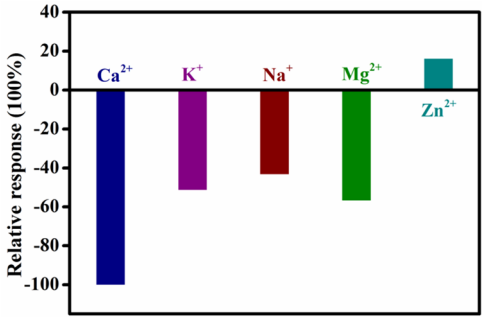

Figure 5. Response of the electrode with the addition of Ca^{2+} and other interfering metal ions at the same concentration.

Ca^{2+} and interfering metal ions at the same concentrations. The response of Ca^{2+} was set as 100% and it is obviously higher than K^+, Na^+, Mg^{2+}, and Zn^{2+} ions. This result indicated the high selectivity of the sensor.

CONCLUSIONS

In this work, self-standing glucose and calcium ion sensors were developed based on the nanoneedles $NiCo_2O_4$ directly deposited on the surface of 3DGF. Besides the outstanding sensitivity, the $NiCo_2O_4$/3DGF electrode also has a low detection limit of 0.38 μM for glucose and 4.45 μM for calcium ion (S/N = 3). The excellent analytical performance of the $NiCo_2O_4$/3DGF electrode can be attributed to the remarkable electrocatalytic activity provided by $NiCo_2O_4$ nanoneedles and the high active surface area and conductivity from 3D graphene. Moreover, the combination of nickel and cobalt species makes nickel cobalt oxide exhibit better performance than that of nickel oxide or cobalt oxide. With the advantages of high sensitivity, good selectivity, low cost, and facial fabrication, the proposed sensor is a promising candidate for other molecules' selective and sensitive detection.

AUTHOR INFORMATION

Corresponding Authors

*E-mail: iamxcdong@njtech.edu.cn (X.C.D.).
*E-mail: iamwhuang@njtech.edu.cn (W.H.).

Notes

The authors declare no competing financial interest.

ACKNOWLEDGMENTS

The project was supported by 973 program (2014CB660808), Key University Science Research Project of Jiangsu Province (15KJA430006), Jiangsu Provincial Founds for Distinguished Young Scholars (BK20130046), the NNSF of China (21275076, 61328401), Program for New Century Excellent Talents in University (NCET-13-0853), Qing Lan Project, Synergetic Innovation Center for Organic Electronics and Information Displays, the Priority Academic Program Development of Jiangsu Higher Education Institutions (PAPD).

REFERENCES

(1) Ross, S.-A.; Gulve, E.-A.; Wang, M. Chemistry and biochemistry of type 2 diabetes. Chemistry and Biochemistry of Type 2 Diabetes. *Chem. Rev.* **2004**, *104*, 1255−1282.

(2) DiSanto, R.-M.; Subramanian, V.; Gu, Z. Recent Advances in Nanotechnology for Diabetes Treatment. *Wires. Nanomed. Nanobi.* **2015**, *7*, 548−564.

(3) Wang, X.-W.; Sun, G.-Z.; Routh, P.; Kim, D.-H.; Huang, W.; Chen, P. Heteroatom-Doped Graphene Materials: Syntheses, Properties and Applications. *Chem. Soc. Rev.* **2014**, *43*, 7067−7098.

(4) Silver, J.; Kilav, R.; Naveh-Many, T. Mechanisms of Secondary Hyperparathyroidism. *Am. J. Physiol.* **2002**, *283*, F367−F376.

(5) Badhulika, S.; Paul, R.-K.; Rajesh; Terse, T.; Mulchandani, A. Nonenzymatic Glucose Sensor Based on Platinum Nanoflowers Decorated Multiwalled Carbon Nanotubes-Graphene Hybrid Electro. *Electroanalysis* **2014**, *26*, 103−108.

(6) Senthilkumar, N.; Babu, K.-J.; Gnana kumar, G.; Kim, A.-R.; Yoo, D.-J. Flexible Electrospun PVdF-HFP/Ni/Co Membranes for Efficient and Highly Selective Enzyme Free Glucose Detection. *Ind. Eng. Chem. Res.* **2014**, *53*, 10347−10357.

(7) Wang, L.; Lu, X.; Ye, Y.; Sun, L.; Song, Y. Nickel-Cobalt Nanostructures Coated Reduced Graphene Oxide Nanocomposite Electrode for Nonenzymatic Glucose Biosensing. *Electrochim. Acta* **2013**, *114*, 484−493.

(8) Jiang, Y.; Yu, S.; Li, J.; Jia, L.; Wang, C. Improvement of Sensitive $Ni(OH)_2$ Nonenzymatic Glucose Sensor Based on Carbon Nanotube/Polyimide Membrane. *Carbon* **2013**, *63*, 367−375.

(9) Heli, H.; Pishahang, J. Cobalt Oxide Nanoparticles Anchored to Multiwalled Carbon Nanotubes: Synthesis and Application for Enhanced Electrocatalytic Reaction and Highly Sensitive Nonenzymatic Detection of Hydrogen Peroxide. *Electrochim. Acta* **2014**, *123*, 518−526.

(10) Song, J.; Xu, L.; Zhou, C.; Xing, R.; Dai, Q.; Liu, D.; Song, H. Synthesis of Graphene Oxide Based CuO Nanoparticles Composite Electrode for Highly Enhanced Nonenzymatic Glucose Detection. *ACS Appl. Mater. Interfaces* **2013**, *5*, 12928−12934.

(11) Gao, Y.; Mi, L.-W.; Wei, W.-W.; Cui, S.-Z.; Zheng, Z.; Hou, H.-W.; Chen, W.-H. Double Metal Ions Synergistic Effect in Hierarchical Multiple Sulfide Microflowers for Enhanced Supercapacitor Performance. *ACS Appl. Mater. Interfaces* **2015**, *7*, 4311−4319.

DOI: 10.1021/acsami.5b06299
ACS Appl. Mater. Interfaces 2015, 7, 21089−21094

(12) Xu, J.; Wang, Q.-F.; Wang, X.-W.; Xiang, Q.-Y.; Liang, B.; Chen, D.; Shen, G.-Z. Flexible Asymmetric Supercapacitors Based upon Co_9S_8 Nanorod//Co_3O_4@RuO_2 Nanosheet Arrays on Carbon Cloth. *ACS Nano* **2013**, *7*, 5453−5462.
(13) Wang, H.; Feng, H.-B.; Li, J.-H. Graphene and Graphene-like Layered Transition Metal Dichalcogenides in Energy Conversion and Storage. *Small* **2014**, *10*, 2165−2181.
(14) Chabi, S.; Peng, C.; Hu, D.; Zhu, Y.-Q. Ideal Three-Dimensional Electrode Structures for Electrochemical Energy Storage. *Adv. Mater.* **2014**, *26*, 2440−2445.
(15) Sun, C.-C.; Yang, J.; Rui, X.-H.; Zhang, W.-N.; Yan, Q.-Y.; Chen, P.; Huo, F.-W.; Huang, W.; Dong, X.-C. MOF-Directed Templating Synthesis of a Porous Multicomponent Dodecahedron with Hollow Interiors for Enhanced Lithium-Ion Battery Anodes. *J. Mater. Chem. A* **2015**, *3*, 8483−8488.
(16) Deng, H.; Shen, W.; Peng, Y.; Chen, X.; Yi, G.; Gao, Z. Nanoparticulate Peroxidase/Catalase Mimetic and its Application. *Chem. - Eur. J.* **2012**, *18*, 8906−8911.
(17) Chen, Z.; Yin, J.-J.; Zhou, Y.-T.; Zhang, Y.; Song, L.; Song, M.; Hu, S.; Gu, N. Dual Enzyme-like Activities of Iron Oxide Nanoparticles and their Implication for Diminishing Cytotoxicity. *ACS Nano* **2012**, *6*, 4001−4012.
(18) Mu, J. S.; Zhang, L.; Zhao, M.; Wang, Y. Co3O4 Nanoparticles as an Efficient Catalase Mimic: Properties, Mechanism and its Electrocatalytic Sensing Application for Hydrogen Peroxide. *J. Mol. Catal. A: Chem.* **2013**, *378*, 30−37.
(19) Cheng, F.-Y.; Shen, J.; Peng, B.; Pan, Y.-D.; Tao, Z.-L.; Chen, J. Rapid Room-Temperature Synthesis of Nanocrystalline Spinels as Oxygen Reduction and Evolution Electrocatalysts. *Nat. Chem.* **2011**, *3*, 79−84.
(20) Hu, L.-F.; Wu, L.-M.; Liao, M.-Y.; Hu, X.-H.; Fang, X.-S. Electrical Transport Properties of Large, Individual $NiCo_2O_4$ Nanoplates. *Adv. Funct. Mater.* **2012**, *22*, 998−1004.
(21) Liang, Y.-Y.; Wang, H.-L.; Zhou, J.-G.; Li, Y.-G.; Wang, J.; Regier, T.; Dai, H. Covalent Hybrid of Spinel Manganese-Cobalt Oxide and Graphene as Advanced Oxygen Reduction Electrocatalysts. *J. Am. Chem. Soc.* **2012**, *134*, 3517−3523.
(22) Jo, M.-R.; Jung, Y.-S.; Kang, Y.-M. Tailored $Li_4Ti_5O_{12}$ Nanofibers with Outstanding Kinetics for Lithium Rechargeable Batteries. *Nanoscale* **2012**, *4*, 6870−6875.
(23) Lu, L.-M.; Li, H.-B.; Qu, F.-L.; Zhang, X.-B.; Shen, G.-L.; Yu, R.-Q. In Situ Synthesis of Palladium Nanoparticle-Graphene Nanohybrids and Their Application in Nonenzymatic Glucose Biosensors. *Biosens. Bioelectron.* **2011**, *26*, 3500−3504.
(24) Zhang, Y.-F.; Ma, M.-Z.; Yang, J.; Su, H.-Q.; Huang, W.; Dong, X.-C. Selective Synthesis of Hierarchical Mesoporous Spinel $NiCo_2O_4$ for High-performance Supercapacitors. *Nanoscale* **2014**, *6*, 4303−4308.
(25) Bai, S.; Shen, X.-P.; Zhu, G.-X.; Li, M.-Z.; Xi, H.-T.; Chen, K. M. In situ Growth of Ni_xCo_{100-x} Nanoparticles on Reduced Graphene Oxide Nanosheets and Their Magnetic and Catalytic Properties. *ACS Appl. Mater. Interfaces* **2012**, *4*, 2378−2386.
(26) Yang, X.-Y.; Zhang, X.-Y.; Ma, Y.-F.; Huang, Y.; Wang, Y.-S.; Chen, Y.-S. Superparamagnetic Graphene Oxide-Fe_3O_4 Nanoparticles Hybrid for Controlled Targeted Drug Carriers. *J. Mater. Chem.* **2009**, *19*, 2710−2714.
(27) Jang, S.; Hwang, E.; Lee, Y.; Lee, S.; Cho, J. H. Multifunctional Graphene Optoelectronic Devices Capable of Detecting and Storing Photonic Signals. *Nano Lett.* **2015**, *15*, 2542−2547.
(28) Chen, Z.-P.; Ren, W.-C.; Gao, L.-B.; Liu, B.-L.; Pei, S.-F.; Cheng, H.-M. Three-Dimensional Flexible and Conductive Interconnected Graphene Networks Grown by Chemical Vapor Deposition. *Nat. Mater.* **2011**, *10*, 424−428.
(29) Liu, Y.-X.; Dong, X.-C.; Chen, P. Biological and Chemical Sensors Based on Graphene Materials. *Chem. Soc. Rev.* **2012**, *41*, 2283−2307.
(30) Maiyalagan, T.; Dong, X.-C.; Chen, P.; Wang, X.-J. Electrodeposited Pt on Three-Dimensional Interconnected Graphene as a Free-Standing Electrode for Fuel Cell Application. *J. Mater. Chem.* **2012**, *22*, 5286−90.
(31) Reina, A.; Jia, X.-T.; Ho, J.; Nezich, D.; Son, H.-B.; Bulovic, V.; Dresselhaus, M.-S.; Kong, J. Large Area, Few-Layer Graphene Films on Arbitrary Substrates by Chemical Vapor Deposition. *Nano Lett.* **2009**, *9*, 30.
(32) Graf, D.; Molitor, F.; Ensslin, K.; Stampfer, C.; Jungen, A.; Hierold, C.; Wirtz, L. Spatially Resolved Raman Spectroscopy of Single- and Few-Layer Graphene. *Nano Lett.* **2007**, *7*, 238−242.
(33) Liu, X.-Y.; Shi, S.-J.; Xiong, Q.-Q.; Li, L.; Zhang, Y.-J.; Tang, H.; Gu, C.-D.; Wang, X.-L.; Tu, J. P. Hierarchical $NiCo_2O_4$@$NiCo_2O_4$ Core/Shell Nanoflake Arrays as High-Performance Supercapacitor Materials. *ACS Appl. Mater. Interfaces* **2013**, *5*, 8790−8795.
(34) Liu, X.-Y.; Zhang, Y.-Q.; Xia, X.-H.; Shi, S.-J.; Lu, Y.; Wang, X.-L.; Gu, C.-D.; Tu, J.-P. Self-Assembled Porous $NiCo_2O_4$ Hetero-Structure Array for Electrochemical Capacitor. *J. Power Sources* **2013**, *239*, 157−163.
(35) Wang, X.; Han, X.-D.; Lim, M.-F.; Singh, N.; Gan, C.-L.; Jan, M.; Lee, P.-S. Nickel Cobalt Oxide-Single Wall Carbon Nanotube Composite Material for Superior Cycling Stability and High-Performance Supercapacitor Application. *J. Phys. Chem. C* **2012**, *116*, 12448−12454.
(36) Dong, X.-C.; Xu, H.; Wang, X.-W.; Huang, Y.-X.; Chan-Park, M.-B.; Zhang, H.; Wang, L.-H.; Huang, W.; Chen, P. 3D Graphene Cobalt Oxide Electrode for High-Per formance Supercapacitor and Enzymeless Glucose Detection. *ACS Nano* **2012**, *6*, 3206−3213.
(37) Zheng, L.; Zhang, J.-Q.; Song, J.-F. Effect of Seven Different Additives on the Properties of MR Fluids. *Electrochim. Acta* **2009**, *54*, 4559−4565.
(38) Zhan, B.-B.; Liu, C.-B.; Chen, H.-P.; Shi, H.-X.; Wang, L.-H.; Chen, P.; Huang, W.; Dong, X.-C. Free-Standing Electrochemical Electrode Based on $Ni(OH)_2$/3D Graphene Foam for Nonenzymatic Glucose Detection. *Nanoscale* **2014**, *6*, 7424−7429.
(39) Ci, S.-Q.; Huang, T.-Z.; Wen, Z.-H.; Cui, S.-M.; Mao, S.; Steeber, D.-A.; Chen, J.-H. Nickel Oxide Hollow Microsphere for Non-Enzyme Glucose Detection. *Biosens. Bioelectron.* **2014**, *54*, 251−257.
(40) Hussain, M.; Ibupoto, Z.-H.; Abbasi, M.-A.; Liu, X.-J.; Nur, O.; Willander, M. Synthesis of Three Dimensional Nickel Cobalt Oxide Nanoneedles on Nickel Foam, Their Characterization and Glucose Sensing Application. *Sensors* **2014**, *14*, 5415−5425.
(41) Zhang, X.; Yu, S.; He, W.-Y.; Uyama, H.; Xie, Q.-J.; Zhang, L.; Yang, F.-C. Electrochemical Sensor Based on Carbon-Supported $NiCoO_2$ Nanoparticles for Selective Detection of Ascorbic Acid. *Biosens. Bioelectron.* **2014**, *55*, 446−451.
(42) Mu, J.-S.; Zhang, L.; Zhao, M.; Wang, Y. Catalase Mimic Property of Co_3O_4 Nanomaterials with Different Morphology and Its Application as a Calcium Sensor. *ACS Appl. Mater. Interfaces* **2014**, *6*, 7090−7098.
(43) Mu, J.-S.; Zhang, L.; Zhao, M.; Wang, Y. Co_3O_4 Nanoparticles as an Efficient Catalase Mimic: Properties, Mechanism and Its Electrocatalytic Sensing Application for Hydrogen Peroxide. *J. Mol. Catal. A: Chem.* **2013**, *378*, 30−37.
(44) Yamaguchi, K.; Mori, K.; Mizugaki, T.; Ebitani, K.; Kaneda, K. Epoxidation of α,β-Unsaturated Ketones using Hydrogen Peroxide in the Presence of Basic Hydrotalcite Catalysts. *J. Org. Chem.* **2000**, *65*, 6897−6903.

DOI: 10.1021/acsami.5b06299
ACS Appl. Mater. Interfaces 2015, 7, 21089−21094